Cell. Mol. Life Sci. (2013) 70:121–136
DOI 10.1007/s00018-012-1061-y

Cellular and Molecular Life Sciences

RESEARCH ARTICLE

The LRRK2 *G2019S* mutant exacerbates basal autophagy through activation of the MEK/ERK pathway

José M. Bravo-San Pedro · Mireia Niso-Santano · Rubén Gómez-Sánchez · Elisa Pizarro-Estrella · Ana Aiastui-Pujana · Ana Gorostidi · Vicente Climent · Rakel López de Maturana · Rosario Sanchez-Pernaute · Adolfo López de Munain · José M. Fuentes · Rosa A. González-Polo

Received: 18 March 2012 / Revised: 29 May 2012 / Accepted: 14 June 2012 / Published online: 8 July 2012

Abstract Mutations in leucine-rich repeat kinase 2 (LRRK2) are a major cause of familial Parkinsonism, and the *G2019S* mutation of LRRK2 is one of the most prevalent mutations. The deregulation of autophagic processes in nerve cells is thought to be a possible cause of Parkinson's disease (PD). In this study, we observed that *G2019S* mutant fibroblasts exhibited higher autophagic activity levels than control fibroblasts. Elevated levels of autophagic activity can trigger cell death, and in our study, *G2019S* mutant cells exhibited increased apoptosis hallmarks compared to control cells. LRRK2 is able to induce the phosphorylation of MAPK/ERK kinases (MEK). The use of 1,4-diamino-2,3-dicyano-1,4-bis[2-aminophenylthio]butadiene (U0126), a highly selective inhibitor of MEK1/2, reduced the enhanced autophagy and sensibility observed in *G2019S* LRRK2 mutation cells. These data suggest that the *G2019S* mutation induces autophagy via MEK/ERK pathway and that the inhibition of this exacerbated autophagy reduces the sensitivity observed in *G2019S* mutant cells.

J. M. Fuentes and R. A. González-Polo contributed equally to this paper.

Electronic supplementary material The online version of this article (doi:10.1007/s00018-012-1061-y) contains supplementary material, which is available to authorized users.

J. M. Bravo-San Pedro · M. Niso-Santano · R. Gómez-Sánchez · E. Pizarro-Estrella · J. M. Fuentes (✉) · R. A. González-Polo (✉)
Departamento de Bioquímica y Biología Molecular y Genética, E. Enfermería y T.O., Centro de Investigación Biomédica en Red sobre Enfermedades Neurodegenerativas (CIBERNED), Universidad de Extremadura, Avda Universidad, s/n, 10003 Cáceres, Spain
e-mail: jfuentes@unex.es

R. A. González-Polo
e-mail: rosapolo@unex.es

J. M. Bravo-San Pedro
e-mail: chemabsp@unex.es

M. Niso-Santano
e-mail: mireianiso@hotmail.com

R. Gómez-Sánchez
e-mail: rubengs@unex.es

E. Pizarro-Estrella
e-mail: epizest@unex.es

A. Aiastui-Pujana · A. Gorostidi
Neuroscience Area, Instituto Biodonostia and CIBERNED, 20014 San Sebastián, Spain
e-mail: ana.aiastui@gmail.com

A. Gorostidi
e-mail: ana.gorostidipagola@osakidetza.net

V. Climent
Departamento de Anatomía y Embriología Humana, Facultad de Medicina, Universidad de Extremadura, 06071 Badajoz, Spain
e-mail: vcliment@unex.es

R. López de Maturana · R. Sanchez-Pernaute
Laboratorio de Células madre y Neurorreparación, Fundación Inbiomed, 20009 San Sebastián, Spain
e-mail: rmaturana@inbiomed.org

R. Sanchez-Pernaute
e-mail: rpernaute@inbiomed.org

A. López de Munain
Centro de Investigación Biomédica en Red sobre Enfermedades Neurodegenerativas (CIBERNED), Instituto Biodonostia, Servicio de Neurología, Hospital Donostia, 20014 San Sebastián, Spain
e-mail: adolfo.lopezdemunainarregui@osakidetza.net

Keywords Autophagy · LRRK2 · G2019S · ERK · Parkinson's disease

Abbreviations

Baf A1	Bafilomycin A1
cDNA	DNA complementary
CMFDA	5-chloromethylfluorescein diacetate
Cyt c	Cytochrome c
SDS-PAGE	Sodium dodecyl sulfate–polyacrylamide gel electrophoresis
EBSS	Earle's balanced salt solution medium
ERK	MAPK/extracellular signal-regulated protein kinase
ERM	Ezrin/radixin/moesin
GAPDH	Glyceraldehyde-3-phosphate dehydrogenase
Ho	Hoechst 33342
LAMP-2	Lysosomal-associated membrane protein 2
LRRK2	Leucine-rich repeat kinase 2
LTR	LysoTracker Red DND99
MAPK	Mitogen-activated protein kinase
MBP	Myelin basic protein
MEK	MAPK/ERK kinase
mTOR	The mammalian target of rapamycin
PBS	Phosphate buffered saline
PCR	Polymerase chain reaction
PD	Parkinson's disease
PI	Propidium iodide
ROS	Reactive oxygen species
U0126	1,4-diamino-2,3-dicyano-1,4-bis [2-aminophenylthio]butadiene
Wt	Wild-type

Introduction

Parkinson's disease (PD) is a neurodegenerative disorder characterized by the progressive loss of dopaminergic neurons in the substantia nigra of the midbrain. Exposure to certain environmental toxins [1], age and genetic predisposition are important factors in the initiation and progression of the disease. Even in sporadic PD, genetic susceptibility likely plays an important role; gene products may interact with certain environmental toxins to block or modify cellular processes, particularly processes related to defense against oxidative stress and mitochondrial function and protein degradation mechanisms such as the ubiquitin proteasome system and autophagy [2, 3].

Leucine-rich repeat kinase 2 (LRRK2) is a protein encoded by the *PARK8* locus. Several mutations throughout the sequence of LRRK2 have been linked to hereditary Parkinsonism [4, 5]. The *G2019S* LRRK2 mutation is the most prevalent and is responsible for 0.5–2 % of sporadic cases of PD and more than 10 % of familial PD cases [6]. The substitution of glycine for serine at position 2019 (*G2019S*) increases the accessibility of the kinase domain to the substrate, which increases the enzyme's capacity for autophosphorylation 2.5-fold and its capacity for substrate phosphorylation threefold [7]. This increase in kinase activity induces a dramatic increase in the toxicity of LRRK2 [8]. In this sense, many studies have associated changes in LRRK2 kinase activity with cellular death processes; thus, the search for physiologic substrates is of great importance. LRRK2-catalyzed phosphorylation of myelin basic protein (MBP) is increased by the *G2019S* LRRK2 mutation [7, 9]. Moesin and tubulin-beta, related proteins that are associated with the cytoskeleton and the cytoplasmic membranes, have also been described as LRRK2 substrates [10]; thus, LRRK2 has been proposed to be a regulator of the cytoskeleton [11]. Initiation factor 4E-binding protein (4E-BP1) has also been postulated as a LRRK2 substrate [12].

In addition, LRRK2 autophosphorylation activity has been reported, and the regulation of the GTPase and kinase activity of LRRK2 depends on this autophosphorylation capacity [13]. A recent study has revealed that Ser2403, Thr1410, and Thr1491 in the Roc domain, like Thr1967 and Thr1969 in the kinase domain, can be phosphorylated by the LRRK2 molecule [14]. Ser910 and Ser935 can also be autophosphorylated and are essential for maintaining the molecule's stability [15, 16].

Some studies have linked the LRRK2 protein to cellular maintenance functions and cell morphology [17]. Moreover, additional studies have investigated interactions between LRRK2 and mitogen-activated kinases (MAPKs), such as extracellular signal-regulated kinase (ERK), Jun N-terminal kinase (JNK) and p38 [18], as well as other proteins involved in PD, such as alpha-synuclein [19] and parkin [20]. LRRK2 is also involved in protein transport through synaptic vesicles [21] and the ubiquitination process [22]. In addition, some studies have associated LRRK2 with autophagy [17].

Highly conserved throughout evolution, autophagy is an intracellular catabolic mechanism by which a cell recycles or degrades damaged proteins and cytoplasmic organelles [23]. Autophagy has been associated with cellular dysfunction in various diseases such as cancer [24], cardiomyopathies [25], and neurodegenerative processes, including those observed in PD [3, 26]. These neurodegenerative processes are associated with the increased formation of autophagic vacuoles in the substantia nigra of patients with PD [27]. Paradoxically, some authors consider autophagy to be a protective process for the cell because it is thought to contribute to the recycling of potentially cytotoxic protein aggregates [28]. However, other authors believe that the autophagic process may play

a role in triggering cell death through the execution of a program for irreversible cellular self-destruction [29].

The regulation of autophagy is complex [30]. The mammalian target of rapamycin (mTOR) protein is one of the most commonly studied repressors of autophagy. mTOR is a protein kinase that is active under favorable cellular conditions and suppresses autophagy by interacting with protein phosphatase 2A (PP2A) [31]. Phosphoinositide 3-kinase (PI3K) class I is also involved in the negative regulation of autophagy through a direct interaction with mTOR. Similar to class I PI3K, NF-kappa-B regulates autophagy through the suppression of mTOR [32]. Bcl-2 inhibits autophagy by inhibiting activation pathways, such as class III PI3K interactions via Beclin-1, and via the protection that Bcl-2 exerts on the mitochondrial membrane of the cell [33]. Among the mechanisms that positively regulate autophagy, the most well known is class III PI3K pathway-dependent Beclin-1, which activates the early stages of autophagosome formation [34]. Some studies have described the production of reactive oxygen species (ROS) [35] or the ERK/MEK route as possible inducers of autophagy [17, 36, 37]. Constitutively active IKK subunits have been found to stimulate autophagy and transduce multiple signals that operate in starvation-induced autophagy, including the phosphorylation of AMPK and JNK1 [38]. The relationship between autophagy and LRRK2 is evident, although it is not known exactly how they interact. Multiple studies have shown interactions between LRRK2 and various proteins involved in the autophagy process. For example, LRRK2 interacts with AMPK/mTOR/ULK1 [39, 40], an important mechanism for cells in situations of metabolic stress. LRRK2 is also important for cytoskeleton maintenance [41], which is essential for autophagy flux [42]. LRRK2 participates in Beclin-1 independent autophagy [43] and is intimately linked to the MEK/ERK pathway [18, 44, 45], which is also involved in the autophagy induction process.

In this study, we investigated the effect of the *G2019S* LRRK2 mutation. We then analyzed the role of the MEK/ERK pathway in these processes because the *G2019S* LRRK2 mutation is known to activate these MAP kinases. Our results indicate that MEK/ERK plays an active role in the increased level of autophagy observed in cells with the *G2019S* LRRK2 mutation.

Materials and methods

Subjects

Skin samples were obtained from three PD patients (*G2019S* group, denoted as GS1–GS3) and four healthy individuals (control group, termed C1–C4) who were undergoing plastic surgery. There were no significant age differences between the control (59.71 ± 17.22 years of age) and *G2019S* groups (65.33 ± 0.55 years of age); the *t* value for this comparison was 0.6. There were also no significant differences in the gender composition of the two participant groups. All subjects gave informed consent using forms approved by the Ethical Committee on the Use of Human Subjects in Research at Donosti Hospital. The three PD patients were diagnosed with familial PD at the Movement Disorders Unit of Donosti Hospital, according to the Gelb criteria [46]. The patients presented with a typical parkinsonian syndrome, and all experienced onset of the disease in their mid-fifties.

Human dermal fibroblast isolation and culture

Skin was collected in RPMI 1640 medium with 2 % penicillin (1,000 U/ml)/streptomycin (10,000 μg/μl) (Invitrogen, Carlsbad, CA, USA). All of the fat tissue was removed with sterilized scissors and a scalpel and washed with fresh medium. Briefly, washed skin was chopped into 2–3 mm^3 fragments and placed on a surface moistened with modified Eagle's medium (MEM) (Invitrogen, Carlsbad, CA, USA) containing 13 % new-born calf serum (Invitrogen, Carlsbad, CA, USA), 0.4 % penicillin/streptomycin and 2 mM L-glutamine (Sigma, St. Louis, MO, USA). The flasks were incubated vertically for 3–6 h at 37 °C with 5 % CO_2. The flasks were then carefully placed horizontally and returned to the incubator at 37 °C with 5 % CO_2. The medium was changed twice a week. Human fibroblasts were cultivated in DMEM (Invitrogen, Carlsbad, CA, USA) containing 10 % FBS (Invitrogen, Carlsbad, CA, USA) and antibiotics. Primary cells were used for all experiments with less than ten passages in vitro.

Reagents and induction of cell death

Confluent cells (80 %) in 75-cm^2 tissue culture flasks were trypsinized, seeded in tissue culture dishes at a concentration of 5 × 10^4 cells/cm^2, and incubated at 37 °C. To analyze the flux of autophagy, the cells were treated with Bafilomycin A1 (Baf A1) (Sigma, St. Louis, MO, USA) for 24 h at a concentration of 100 nM to block autophagy and were cultivated with Earle's balanced salt solution medium (EBSS) (Sigma, St. Louis, MO, USA) for 24 h to induce autophagy. To analyze the effect of MEK/ERK inhibition, the cells were treated with 1,4-diamino-2,3-dicyano-1,4-bis[2-aminophenylthio] butadiene (U0126) for 24 h at a concentration of 20 μM.

Flow cytometry

To observe apoptosis-associated changes by cytofluorometry, we used 3,3-dihexyloxacarbocyanine iodide [$DiOC_6$(3), 40 nM] to quantify the mitochondrial transmembrane

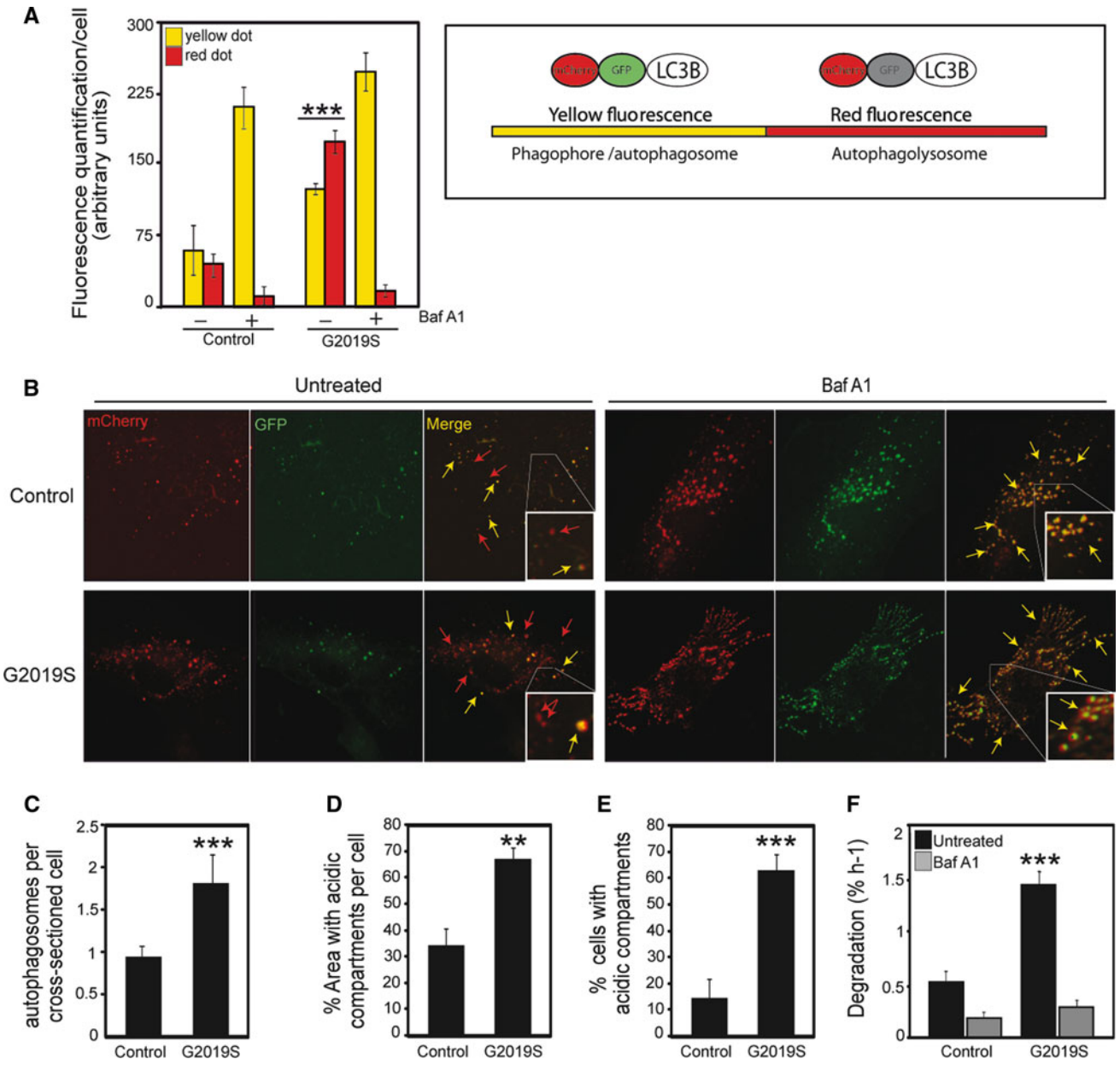

Fig. 1 Detection of autophagy in the control and G2019S fibroblast groups. **a**, **b** Control and mutant fibroblasts were transfected with pDest-mCherry-GFP-LC3B. The number of yellow (autophagosomes) or red vesicles (autophagolysosomes) was quantified. The frequency of the measured changes is presented in **a**, and representative images are shown in **b** [obtained from the C1 (control) and GS1 (G2019S) cell lines]. Data are expressed as the mean ± SEM of all cell lines within each group, control (C1–C4) and G2019S (GS1–GS3), counted in 200 cells per condition (***$p \leq 0.001$ between the untreated control and G2019S groups). **c** Electron microscopy images of the representative cells are shown in Fig. S4. Data represent the mean ± SEM values of the number of autophagosomes per cross-sectioned cell counted in ten cells per condition, control (C1–C4) and G2019S (GS1–GS3) (**$p \leq 0.01$ between the control and *G2019S* groups). **d**, **e** *G2019S* LRRK2 mutants yield a greater number of cells with an accumulation of acidic compartments. Fibroblasts were stained with CMFDA to observe the presence of acidic compartments as indicated in the "Materials and methods" section. Acidic compartments are visualized as holes. Representative microphotographs are depicted in Fig. S5. The data represent the mean ± SEM values of area occupied by acidic compartments per cell counted in 200 cells per condition, control (C1–C4) and G2019S (GS1–GS3) (**d**) and % of cells with acidic compartments, counted in 200 cells per condition (**e**) (***$p \leq 0.001$, **$p \leq 0.01$ between the control and G2019S groups). **f** Study of protein degradation in control and mutant fibroblasts. The protein half-life was determined by pulse-chasing with radioactive valine as indicated in the "Materials and methods" section. The data represent the mean ± SEM of the individuals within each group, control (C1–C4) and G2019S (GS1–GS3), in the presence or absence of Baf A1 (***$p \leq 0.001$ between the untreated control and G2019S groups)

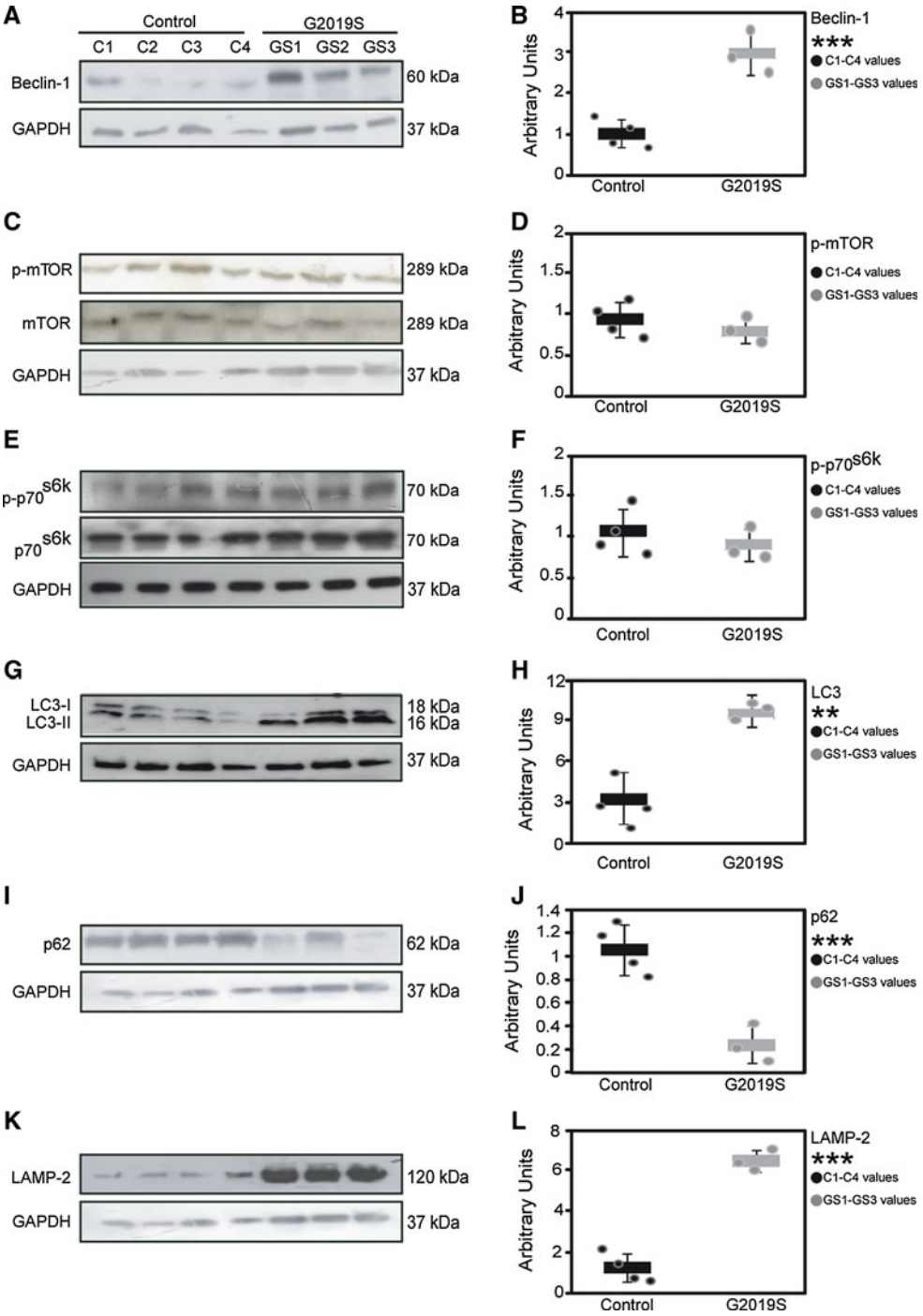

Fig. 2 Western-blot analyses of autophagy-related proteins. Western-blot analysis showing differences in autophagy proteins in the control and *G2019S* LRRK2 mutant fibroblasts. Western blots were probed for all cell lines within each group, control (C1–C4) and G2019S (GS1–GS3), with antibodies against Beclin-1 (**a**), p-mTOR and mTOR (**c**), p-p70^{S6K} and p70^{S6K} (**e**), LC3-I/II (**g**), p62 (i), LAMP-2 (**k**), and GAPDH (used as a loading control under the same conditions). **b** (Beclin-1), **d** (p-mTOR), **f** (p-p70^{S6K}), **h** (LC3), **j** (p62) and **l** (LAMP-2) show the densitometry of each band, expressed in arbitrary units for each Western-blot analysis. *Horizontal bars* represent the mean ± SEM of all cell lines within each group, control (C1–C4) and G2019S (GS1–GS3), and individual values are represented by *points* (***$p \leq 0.001$, **$p \leq 0.01$ between the control and G2019S groups)

potential, annexin V labeled with fluorescein isothiocyanate (FITC) (all from Molecular Probes, Eugene, OR, USA) to assess phosphatidylserine exposure and propidium iodide (PI, 1 μg/ml) to identify cells with permeabilized membranes. The annexin-positive cells were considered to be apoptotic. Hydroethidine (HE, 10 μM) was used to determine superoxide anion generation. After the different experimental conditions were established, the cells were trypsinized and labeled with fluorochromes at 37 °C, followed by cytofluorometric analysis with a FACS Scan (Becton–Dickinson, Franklin Lakes, NJ, USA).

Immunofluorescence

The cells were cultured on coverslips pre-treated with poly-L-lysine. After the experimental conditions were established, the cells were fixed with paraformaldehyde (4 % wt/vol) and then treated for the detection of cytochrome c

(Cyt c) and lysosomal-associated membrane protein 2 (LAMP-2) (Santa Cruz Biotechnology, Santa Cruz, CA, USA), activated caspase-3 and LC3B (Cell Signaling Technology, Beverly, MA, USA). Staining patterns were identified with an anti-mouse or anti-rabbit Alexa-Fluor conjugated immunoglobulin as appropriate (Molecular Probes, Eugene, OR, USA). The cells were counterstained with Hoechst 33342 (Ho) (2 μM; Sigma, St. Louis, MO, USA) before mounting. To visualize acidic compartments, the cells were stained with 5-chloromethylfluorescein diacetate (CMFDA) (Invitrogen, Carlsbad, CA, USA). Results were analyzed as % area with acidic compartments per cells and % cells with acidic compartment (number of cells in which at least 50 % of the cytoplasmic area was occupied by "black holes"). The staining was analyzed with ImageJ software. To visualize lysosomes, the cells were stained with LysoTracker Red DND99 (LTR) (Invitrogen, Carlsbad, CA, USA). After treatment, cells were stained with CMFDA for 30 min at 37 °C and LTR for 15 min at 37 °C. Fluorescence was analyzed with an Olympus IX51 microscope equipped with a DC300F camera (Olympus España, S.A.U., Barcelona, Spain).

Western-blot analysis

The cells were lysed in a buffer containing 50 mM Tris–HCl, pH 6.8, 10 % glycerol and 2 % SDS, heated at 95 °C for 10 min and stored at −80 °C until Western blotting was performed. Equal amounts of protein (40 μg/condition) were resolved by 6–12 % SDS-gel electrophoresis and transferred to polyvinylidene fluoride (PVDF) membranes according to a partially modified conventional protocol [47]. The procedure for immunodetection included transfer and blocking of the membrane with TTBS (10 mM Tris HCl pH 7.5, 150 mM NaCl and 0.2 % Tween-20) containing 10 % non-fat dry milk. The membranes were then incubated with the corresponding primary antibodies: glyceraldehyde-3-phosphate dehydrogenase (GAPDH) from Chemicon (Chandlers Ford, UK), Atg5, p-44/42 MAPK ERK1/2 (Thr202/Tyr204), MAPK ERK1/2, p-mTOR (Ser2448), mTOR, p-p70^{S6K} (Thr389, Thr421/Ser424), p70^{S6K}, LAMP-2, p-ezrin (Thr567)/radixin (Thr564)/moesin (Thr558), ezrin/radixin/moesin from Cell Signaling (Beverly, MA, USA), Beclin-1 from Santa Cruz Biotechnology (Santa Cruz, CA, USA), LC3 and cathepsin B from Sigma (St. Louis, MO, USA), p62 from BD Biosciences, and LRRK2 from MJFF (C81-8 from Epitomics). The membranes were subsequently incubated with peroxidase-conjugated secondary antibodies. The detection of bound antibodies was visualized by chemiluminescence using the ECL-plus reagent (GE Healthcare, Bucks, UK). Quantification was conducted with ImageJ software using GAPDH or nonphosphorylated forms as loading controls.

Fig. 3 Effects of starvation in fibroblasts with or without the *G2019S* LRRK2 mutation. **a**, **b** Detection of apoptotic events by immunofluorescence. Fibroblasts cultured on poly-L-lysine-treated coverslips were exposed to nutrient deprivation with EBSS medium for 24 h followed by fixation and immunostaining for active caspase-3 (*green*) and staining with Hoechst 33342 to visualize nuclear chromatin condensation (*blue*). The frequency of the measured changes is presented in **b**, and representative images are shown in **a** [obtained from the C1 (control) and GS1 (G2019S) cell lines]. The *scale bar* represents 10 μm. Data are expressed as the mean ± SEM of all cell lines within each group, control (C1–C4) and G2019S (GS1–GS3) (***$p \leq 0.001$, **$p \leq 0.01$, *$p \leq 0.05$ between the treated and untreated cells). **c** Detection of PI-positive cells. Fibroblasts were treated as in **a**, followed by staining with PI to determine the viable cells. Data are expressed as the mean ± SEM of all cell lines within each group, control (C1–C4) and G2019S (GS1–GS3) (***$p \leq 0.001$, *$p \leq 0.05$ between the treated and untreated cells). **d–j** Autophagy exacerbation mediated by EBSS in fibroblasts with or without the *G2019S* mutation. **d** Detection of acidic compartments and lysosomal accumulation after starvation. Fibroblasts cultured on poly-L-lysine-treated coverslips were exposed to nutrient deprivation for 24 h followed by staining with CMFDA (*green*) to observe the presence of acidic compartments, and LTR to observe lysosomal swelling, as indicated in the "Materials and methods" section. Acidic compartments are visualized as *holes*. Data are expressed as the mean ± SEM of all cell lines within each group, control (C1–C4) and G2019S (GS1–GS3) (***$p \leq 0.001$, *$p \leq 0.05$ between the treated and untreated cells). **e–j** Western-blot analysis showing the effects of starvation on autophagy in both fibroblast groups. **e** Representative blot of the C1 and GS1 cell lines probed with antibodies against p-mTOR, mTOR, LC3-I/II, p62, LAMP-2, and cathepsin B. GAPDH expression was used as a loading control under the same conditions. **f** (mTOR), **g** (LC3), **h**(p62), **i** (LAMP-2), and **j** (cathepsin B) show the densitometry of each band, expressed in arbitrary units for each Western-blot analysis (***$p \leq 0.001$, *$p \leq 0.05$ between the treated and untreated cells)

Transient transfection plasmid DNA

We used plasmid pDest-mCherry-GFP-LC3B were kindly provided by Dr. Johansen Terje (Molecular Cancer Research group, Institute of Medical Biology. University of Tromsø, Norway) for transient transfection. Fibroblasts were plated in six-well cell culture plates 1 day prior to transfection and transfected with plasmid using the Lipofectamine 2000 reagent (Invitrogen, Carlsbad, CA, USA) according to the manufacturer's recommendations. After 5 h, the transfection medium was replaced with fresh culture medium, and the cells were incubated for another 24 h prior to different treatments. Fluorescence was analyzed with an Olympus IX51 microscope equipped with a DC300F camera (Olympus España, S.A.U., Barcelona, Spain). The staining was analyzed with ImageJ software.

RNA interference

RNA interference was performed by transient transfection of cells with siRNA (10 μM) against the designated genes using Lipofectamine 2000. Human Atg5 siRNA and

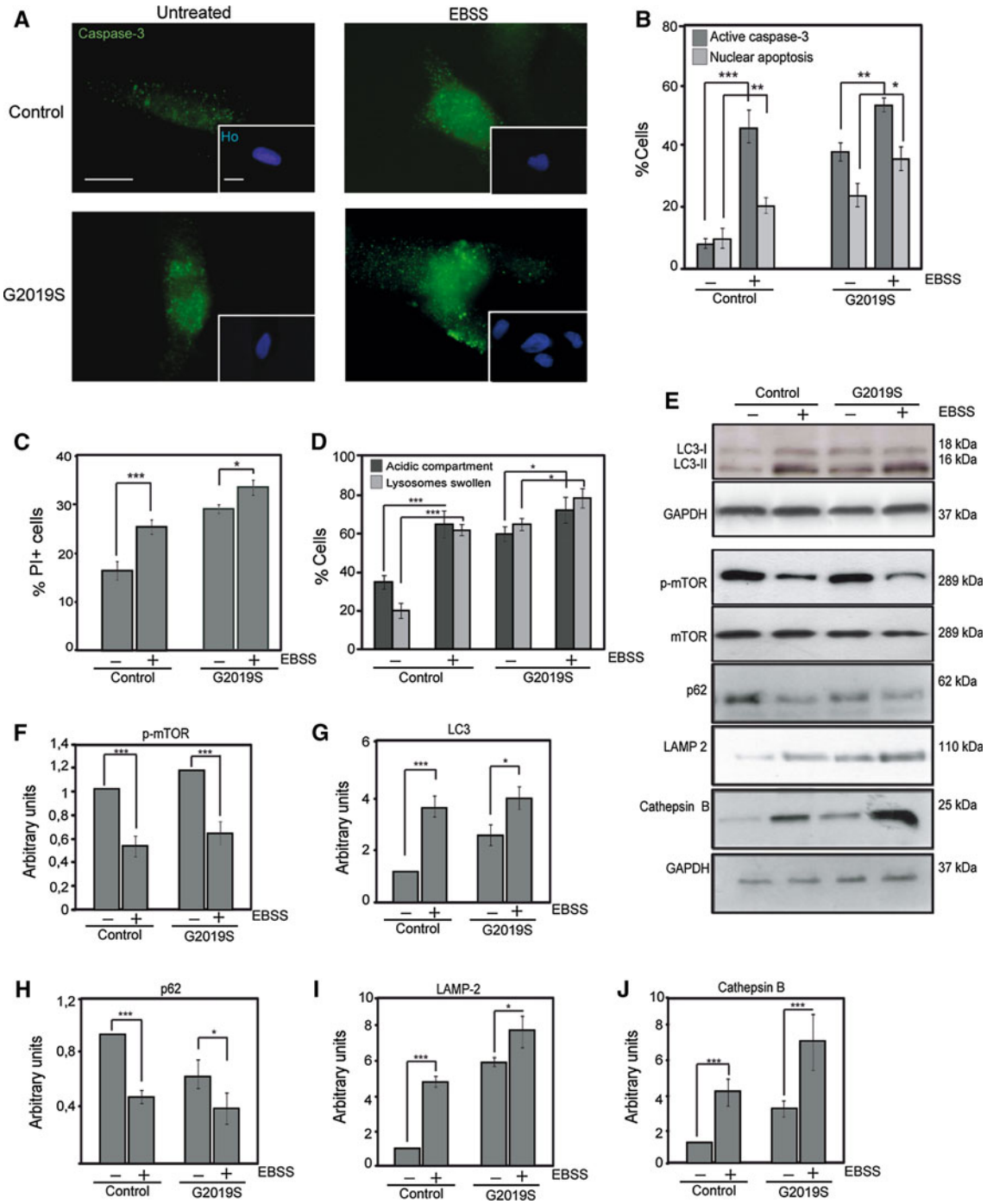

LRRK2 siRNA was obtained from Cell Signaling (Beverly, MA, USA).

Transmission electron microscopy (TEM)

Ultrastructural examinations were conducted in both control and *G2019S* LRRK2 mutant fibroblasts. For this purpose, smaller fragments (~2 mm) were cut from biopsy samples prior to formalin fixation. These samples were fixed in 1.0 % paraformaldehyde/1.5 % glutaraldehyde in 0.05 M cacodylate buffer (pH 7.4) for 2 h at 4 °C, post-fixed in 1 % osmium tetroxide, dehydrated, and embedded in Durcupan (Fluka A.G., Buchs, Switzerland). Semi-thin 1-μm-thick sections were stained with Toluidine Blue 0 (Sigma-Aldrich, Cedex, France), and ultra-thin sections of selected fields were examined with a Jeol JEM-1010 electron microscope (Jeol Ltd., Tokyo, Japan) after staining with uranyl acetate and lead citrate.

Analysis of protein degradation

Human fibroblasts were incubated with 0.2 mCi/ml L-[^{14}C] valine (GE Healthcare) for 24 h at 37 °C. Unincorporated radioisotope was removed by washing the cells three times with PBS (pH 7.4). The cells were then incubated in DMEM in the presence of 10 mM cold valine in the presence or absence of Baf A1 (prechase period). Subsequently, the medium was replaced by the appropriate fresh medium for 4 h (chase period). The cells and radiolabeled proteins from the medium were precipitated with trichloroacetic acid (TCA) at a final concentration of 10 % (vol/vol). The precipitated proteins were separated from the soluble radioactive fraction by centrifugation at 600 × *g* for 20 min and then dissolved in 1 ml of 0.2 N NaOH. The rate of protein degradation was calculated by determining the ratio of acid-soluble radioactivity recovered from both the cells and the medium to the radioactivity of trichloroacetic acid-precipitated proteins obtained from both the cells and the medium, respectively [48].

Gel electrophoresis

PCR products and restriction analyses were visualized by electrophoresis in 2 % or 3 % (wt/vol) agarose gels (Bio-Rad, Hercules, CA, USA). Electrophoresis was performed in 0.5 % Tris–borate-EDTA buffer. The gels were stained with 0.5 µl/ml ethidium bromide (Bio-Rad, Hercules, CA, USA), visualized by ultraviolet transillumination and photographed with a GEL-DOC 2000 system (Bio-Rad, Hercules, CA, USA).

Statistical analysis

Student's *t* test was used for two-group comparisons (control and G2019S or treated and untreated conditions). Results were considered significant when the probability of their occurrence by chance alone was less than 5 %. The data were evaluated with the SPSS ver. 19.0 (SPSS Inc., Chicago, IL) software. Each experiment was repeated at least three times.

Results

The presence of the *G2019S* LRRK2 mutation does not affect the expression level of the LRRK2 protein but significantly increases LRRK2 kinase activity in fibroblasts

The first step in analyzing the role of the *G2019S* LRRK2 mutation in autophagy in human fibroblasts was to confirm the presence or absence of the mutation. The analysis of the LRRK2 PCR products, which were amplified from cDNA or genomic DNA, before and after restriction endonuclease digestion with SfcI confirmed the presence of the mutation in the *G2019S* fibroblasts (Fig. S1 A and B). However, the *G2019S* LRRK2 mutation was identified in the G2019S fibroblast group by direct sequencing (Fig. S1 C). The expression levels of LRRK2 in these fibroblasts were then determined. In agreement with recent studies, the presence of the *G2019S* LRRK2 mutation in the fibroblasts did not affect LRRK2 mRNA expression [49], as determined by qPCR (Fig. S2 A), or protein expression, as determined by Western blotting with a commercial antibody against LRRK2 (Fig. S2 B and C). Therefore, we investigated the LRRK2 kinase activity levels in fibroblasts with or without the *G2019S* LRRK2 mutation. As observed previously [7, 9], kinase activity levels were higher in fibroblasts with the *G2019S* LRRK2 mutation (Fig. S3 A and B). This result was corroborated by Western-blot analysis, which demonstrated that the phosphorylation levels of the LRRK2 substrate ezrin/radixin/moesin (ERM) were higher in *G2019S* LRRK2 fibroblasts than in control fibroblasts (Fig. S3 C and D). We also showed that this phosphorylation was due to LRRK2 because LRRK2 knockdown reverses the increase in phosphorylated ERM caused by the *G2019S* LRRK2 mutation (Fig. S3 E and F).

Fibroblasts with the *G2019S* LRRK2 mutation exhibit higher autophagic activity levels than control fibroblasts

We next investigated the role of autophagy in control fibroblasts and those from individuals with the *G2019S* LRRK2 mutation. Previous studies have shown that LRRK2 plays an important role in regulating autophagy [50], as demonstrated in SH-SY5Y human neuroblastoma cells with the *G2019S* mutation [17].

We tested the autophagosome-lysosome fusion efficiency. We expressed LC3B-GFP-mCherry in human fibroblasts with or without the *G2019S* LRRK2 mutation under basal conditions and with inhibitor of autophagy process (Baf A1). We observed an increase in number of yellow-fluorescence vesicles (autophagosomes) and red-fluorescence (autophagolysosomes) in mutant cells as compared with that in control cells. By inhibiting the formation of autophagolysosome (in the presence of Baf A1), we observed an increase of yellow fluorescence (autophagosomes) and decrease of red fluorescence (autophagolysosomes) in both cell types (Fig. 1a, b). The analysis of these cells by transmission electron microscopy (representative images shown in Fig. S4) verified the existence of a double membrane in the vacuoles and higher number of autophagosomes in *G2019S* LRRK2 mutant cells (Fig. 1c). We also found that mutant fibroblasts

exhibited a significant increase in the presence of acidic compartments (representative images shown in Fig. S5) compared to cells without the mutation (Fig. 1d, e). Moreover, the quantification of protein turnover revealed a threefold increase in protein turnover in the cells carrying the mutation. To verify the relationship between higher levels of protein degradation and increased levels of autophagy, both cell types were treated with the autophagy inhibitor Baf A1. A significant decrease in protein degradation levels was found in both cell types after treatment with this agent (Fig. 1f). Similarly, Western blotting revealed the accumulation of the autophagosome marker LC3-II (Fig. 2g, h), which was correlated with an increase in p62 degradation (Fig. 2i, j). Moreover, we observed increased levels of Beclin-1 protein (Fig. 2a, b) and LAMP-2 (Fig. 2k, l) in fibroblasts with the *G2019S* LRRK2 mutation compared to fibroblasts without the mutation. By contrast, we detected no differences between control and *G2019S* LRRK2 fibroblasts in the phosphorylation (Ser2448) status of mTOR (Fig. 2c, d) or in the degree of substrate ($p70^{S6K}$) binding (Fig. 2e, f).

Effects of starvation on fibroblasts with or without the *G2019S* LRRK2 mutation

Nutrient starvation is a well-characterized strategy to induce autophagy. During starvation, the mTOR protein, a nutrient-responsive kinase, is dephosphorylated and fails to inhibit autophagy downstream target and this is, indeed, stimulating the process [51]. We analyzed the effects of nutrient deprivation with the use of EBSS for 24 h in fibroblasts with or without the *G2019S* LRRK2 mutation. As shown in Fig. 3, nutrient starvation caused a significant increase in apoptotic cell death in both cell types. This finding was corroborated by the immunofluorescent analysis of two parameters of apoptotic death (caspase-3 activation and nuclear condensation) (Fig. 3a, b) and with a cytofluorometric assay with a PI stain (Fig. 3c).

To investigate the starvation-induced changes in autophagy levels observed in fibroblasts, the accumulation of acidic compartments in the cytoplasm was determined by CMFDA staining at 10 μM concentration. Lysosomal swelling was observed by LTR staining, at 1 mM

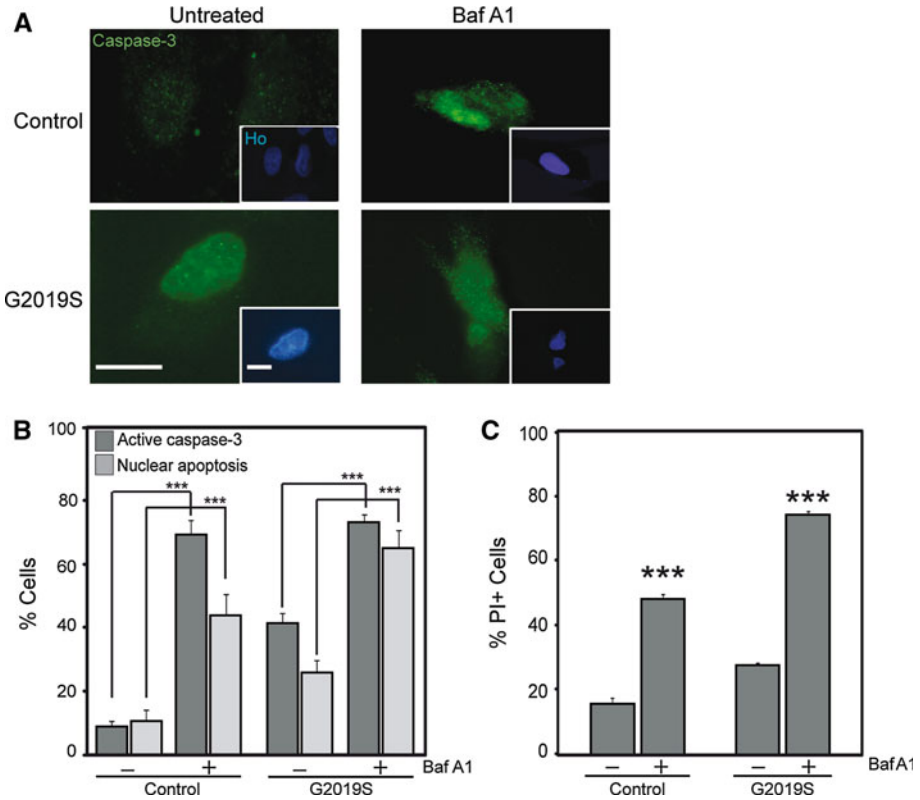

Fig. 4 Effects of treatment with bafilomycin A1 in fibroblasts with or without the *G2019S* LRRK2 mutation. **a**, **b** Apoptotic events were detected by immunofluorescence. Fibroblasts cultured on poly-L-lysine-treated coverslips were treated with Baf A1 (100 nM) for 24 h followed by fixation and immunostaining for active caspase-3 (*green*) and Ho staining for nuclear chromatin condensation (*blue*). The frequency of the measured changes is presented in **b**, and representative images are shown in **a** [obtained from the C3 (control) and GS1 (G2019S) cell lines]. The *scale bar* represents 10 μm. Data are expressed as the mean ± SEM of all cell lines within each group, control (C1–C4) and G2019S (GS1–GS3) (***$p \leq 0.001$ between the treated and untreated cells). **c** Detection of PI-positive cells. Fibroblasts were treated as in **a**, followed by staining with PI to determine the viable cells. Data are expressed as the mean ± SEM of all cell lines within each group, control (C1–C4) and G2019S (GS1–GS3) (***$p \leq 0.001$ between the treated and untreated cells)

concentration in fibroblasts exposed to starvation. Treatment with EBSS increased the number of cells with acidic compartments and the intensity of LTR staining in control fibroblasts (Fig. 3d). These findings were correlated with an accumulation of LC3-II in cells exposed to starvation (Fig. 3e, g) and accumulations of lysosomal-like LAMP-2 protein (Fig. 3e, i) and cathepsin B (Fig. 3e, j). As expected, the increase in autophagy was accompanied by a decrease in p62 protein levels (Fig. 3e, h). Moreover, treatment with EBSS caused a significant dephosphorylation of mTOR in both control and mutant fibroblasts (Fig. 3e, f).

Effects of bafilomycin A1 treatment in fibroblasts with or without the *G2019S* LRRK2 mutation

We analyzed the effects of Baf A1, a potent and specific inhibitor of vacuolar H^+ ATPase (V-ATPase), on the process of autophagy in fibroblasts. Baf A1 blocks the fusion of autophagosomes with lysosomes, preventing the degradation of the autophagosome content [52]. As shown in Fig. 4, Baf A1 exposure significantly increased cell death in control and *G2019S* LRRK2 mutant fibroblasts (Fig. 4c). Under these conditions, caspase-3 activation and nuclear fragmentation were also exacerbated (Fig. 4a, b).

We analyzed the accumulation of acidic compartments in the cytoplasm by CMFDA staining and observing the intensity of LTR staining in fibroblasts exposed to Baf A1. As demonstrated in Fig. 5, treatment with Baf A1 increased the number of cells with acidic compartments in all fibroblasts. Additionally, the intensity of LTR staining in control and mutant fibroblasts was completely inhibited in the presence of Baf A1 (Fig. 5a, b). These results were correlated with the accumulation of LC3B puncta formation in cells exposed to Baf A1, as determined by immunofluorescence (Fig. 5c, d), and the accumulation of LC3-II observed by Western blotting (Fig. 5e, f). The accumulation of the lysosomal protein LAMP-2 was also demonstrated by immunofluorescence (Fig. 5c, d) and Western blotting (Fig. 5e, h). However, Baf A1 treatment abolished cathepsin B levels (Fig. 5e, i). As expected, inhibition of autophagy was accompanied by an increase in p62 protein levels in control and *G2019S* mutant fibroblasts (Fig. 5e, g).

MEK/ERK is essential to the autophagy effects induced by the *G2019S* LRRK2 mutation and the increased sensitivity of these cells

To investigate the importance of the MEK/ERK route in the exacerbated autophagy levels observed in the fibroblasts with the *G2019S* LRRK2 mutation, the phosphorylation status of ERK1/2 was determined by Western blotting at the basal level and after treatment with U0126. As demonstrated in Fig. 6, Western blotting revealed higher levels of ERK1/2 phosphorylation (Thr202/Tyr204) (the active form of the direct substrate of MEK1/2) in cells with the *G2019S* LRRK2 mutation at basal levels (Fig. 6a, b). Treatment with a pharmacological inhibitor of MEK/ERK, such as U0126, significantly reduced the levels of ERK1/2 phosphorylation (upper portion of Fig. 6k). To evaluate whether reduced ERK1/2 phosphorylation levels induce a decrease in autophagy levels, we analyzed the accumulation of acidic compartments in the cytoplasm with CMFDA staining after U0126 treatment in cells with and without the *G2019S* LRRK2 mutation. Treatment with U0126 increased the number of cells with acidic compartments in control cells. However, in cells with the *G2019S* LRRK2 mutation, the number of cells with acidic compartments was reduced significantly (Fig. 6c, d). This result was correlated with LC3-II level changes after U0126 treatment (Fig. 6e, f), including accumulation in control cells and less accumulation in *G2019S* LRRK2 mutant cells. Treatment with U0126 also changes the cell death levels and increases apoptotic hallmarks in control cells but reduces these levels in mutant cells (Fig. 6k). Therefore, the use of U0126 appeared to reduce both autophagy and sensitivity in *G2019S* cells, but it was unclear whether inhibition of MEK/ERK is responsible for the decrease in sensitivity of *G2019S* LRRK2 mutation

Fig. 5 Autophagy inhibition mediated by bafilomycin A1 in fibroblasts with or without the *G2019S* LRRK2 mutation. **a**, **b** Detection of acidic compartments and lysosomal accumulation after Baf A1 treatment. Fibroblasts cultured on poly-L-lysine-treated coverslips were treated with Baf A1 (100 nM) for 24 h, followed by staining with CMFDA (*green*) to observe the presence of cytoplasmic vacuoles, LTR to observe lysosome swelling, as indicated in the "Materials and methods" section. Acidic compartments are visualized as holes. Representative microphotographs are depicted in **a** [obtained from the C1 (control) and GS2 (G2019S) cell lines], and quantitative data are analyzed in **b**. The *scale bar* represents 10 μm. Data are expressed as the mean ± SEM of all cell lines within each group, control (C1–C4) and G2019S (GS1–GS3) (***$p \leq 0.001$ between the treated and untreated cells). **c**, **d** Detection of the puncta formation of LC3B and determination of the expression levels of LAMP-2 by immunostaining after Baf A1 treatment. Fibroblasts cultured on poly-L-lysine-treated coverslips were treated as in **a**, followed by fixation and immunostaining for LC3B (*green*), LAMP-2 (*red*). Representative microphotographs are depicted in **d** [obtained from the C1 (control) and GS1 (G2019S) cell lines], and quantitative data are analyzed in **c**. The *scale bar* represents 10 μm. Data are expressed as the mean ± SEM of all cell lines within each group, control (C1–C4) and G2019S (GS1–GS3) (***$p \leq 0.001$ between the treated and untreated cells). **e**–**i** Western-blot analysis showing the effects of Baf A1 on autophagic proteins. **e** Representative blots probed in C1 and GS1 cell lines, with antibodies against LC3, p62, LAMP-2, cathepsin B, and GAPDH (used as a loading control under the same conditions). **f** (LC3), **g** (p62), **h** (LAMP-2), and **i** (Cathepsin B) show the densitometry of each band, expressed in arbitrary units for each Western-blot analysis (***$p \leq 0.001$ between the treated and untreated cells)

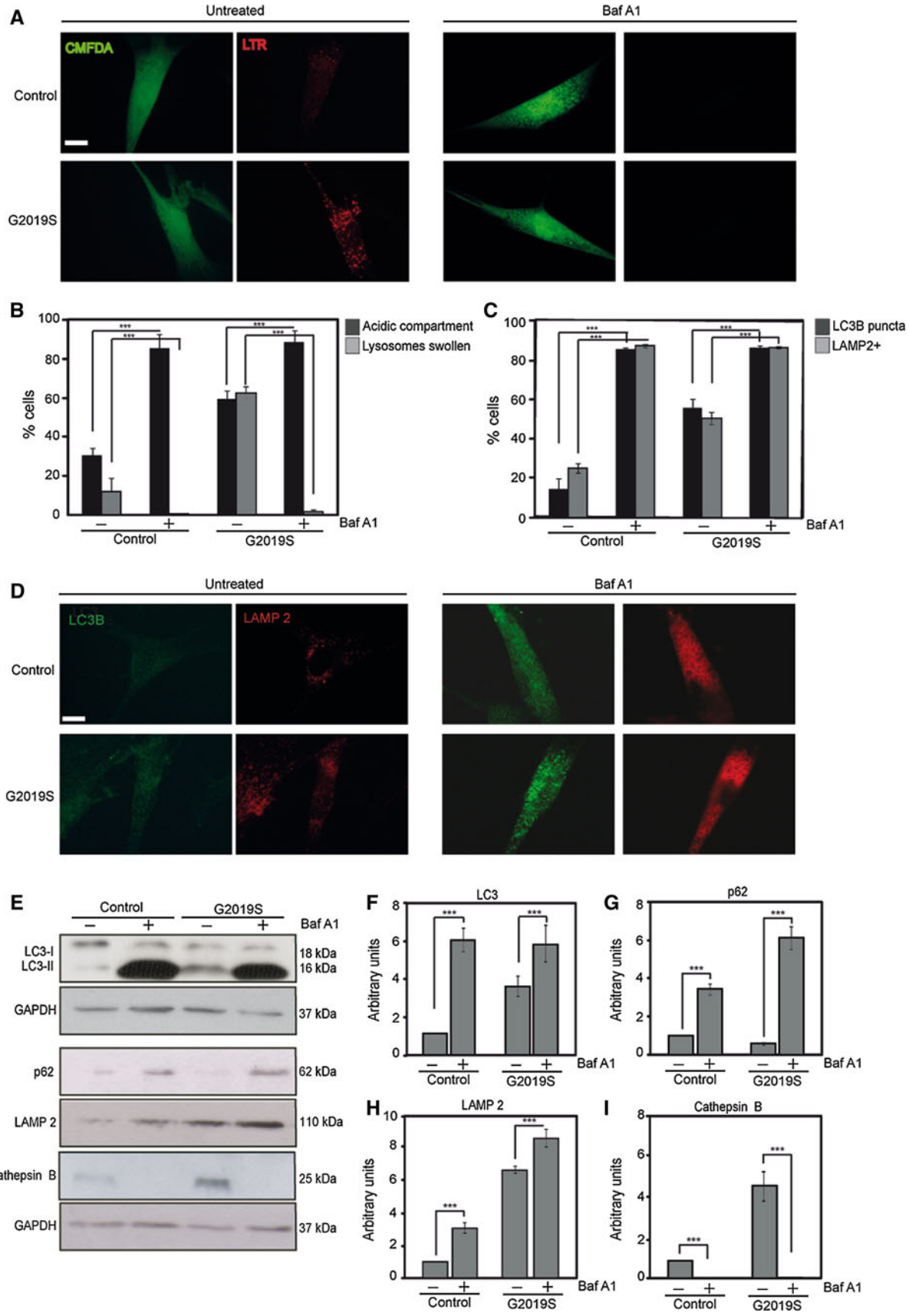
A
Untreated
Baf A1
CMFDA
LTR
Control
G2019S
B
Acidic compartment
Lysosomes swollen
% cells
Control
G2019S
Baf A1
C
LC3B puncta
LAMP2+
% cells
Control
G2019S
Baf A1
D
Untreated
Baf A1
LC3B
LAMP 2
Control
G2019S
E
Control
G2019S
Baf A1
LC3-I
LC3-II
18 kDa
16 kDa
GAPDH
37 kDa
p62
62 kDa
LAMP 2
110 kDa
Cathepsin B
25 kDa
GAPDH
37 kDa
F
LC3
Arbitrary units
Control
G2019S
Baf A1
G
p62
Arbitrary units
Control
G2019S
Baf A1
H
LAMP 2
Arbitrary units
Control
G2019S
Baf A1
I
Cathepsin B
Arbitrary units
Control
G2019S
Baf A1

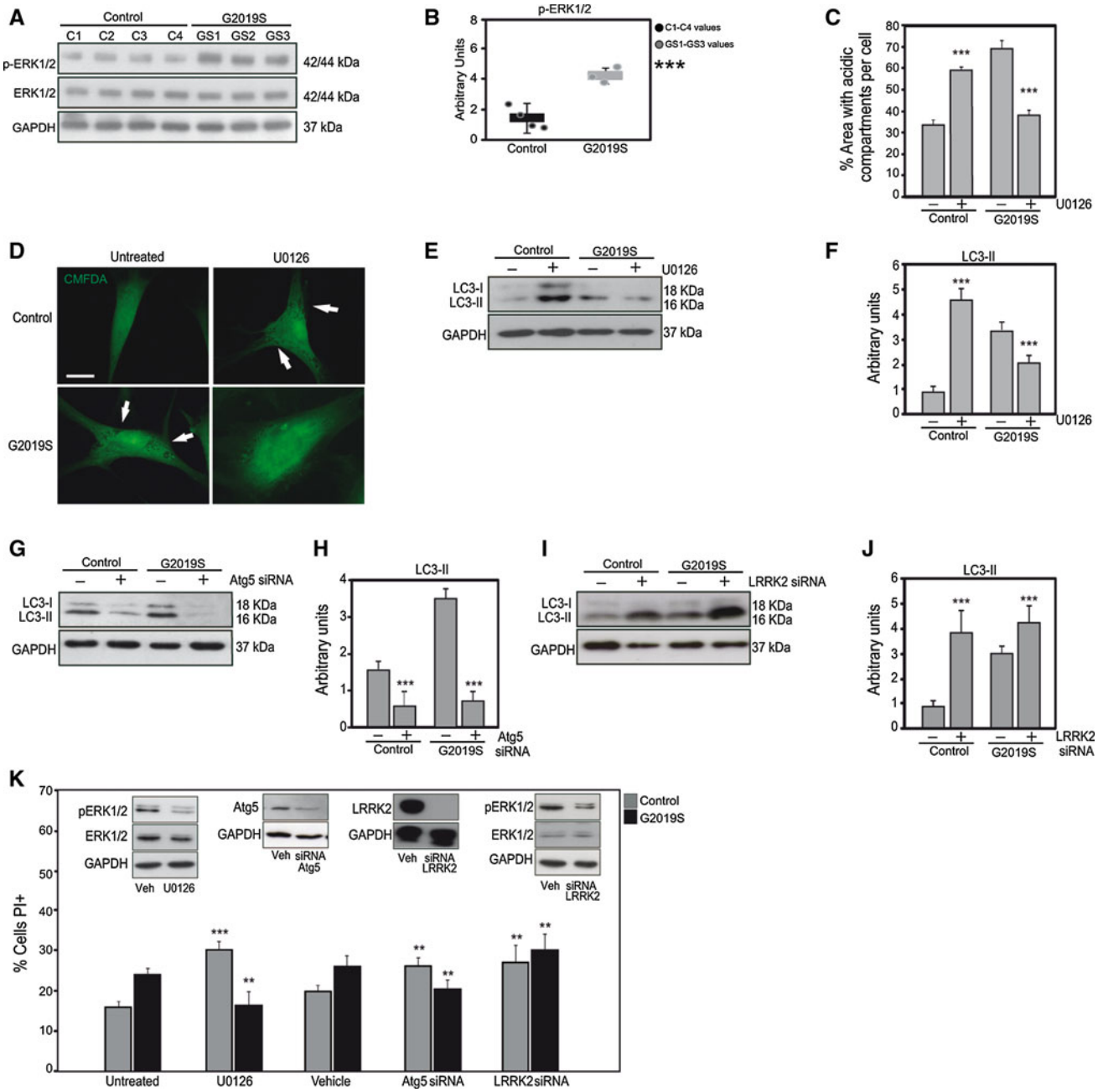

Fig. 6 MEK/ERK inhibition reduces autophagy and sensitivity observed in cells with the *G2019S* LRRK2 mutation. **a**, **b** Western-blot analyses of the phosphorylation levels of the MAPK/ERK protein (p-ERK 1/2) under basal conditions. **a** Western blots probed in all cell lines within each group, control (C1–C4) and G2019S (GS1–GS3), with antibodies against p-ERK1/2, ERK1/2 and GAPDH (used as loading controls under the same conditions). **b** The densitometry of each band, expressed in arbitrary units for Western-blot analysis of **a**. *Horizontal bars* represent the mean ± SEM of all cell lines within each group, control (C1–C4) and G2019S (GS1–GS3), and individual values are represented by *points* (***$p \leq 0.001$ between control and G2019S groups). **c**, **d** Detection of acidic compartments after U0126 treatment (20 μM). Fibroblasts cultured on poly-L-lysine-treated coverslips were exposed to U0126 for 24 h followed by staining with CMFDA (*green*) to observe the presence of acidic compartments, as indicated in the "Materials and methods" section. Acidic compartments are visualized as holes. Representative microphotographs are depicted in **d** [obtained from the C1 (control) and GS2 (G2019S) cell lines]. The *scale bar* represents 10 μm. Quantitative data are presented in **c**. Data are expressed as the mean ± SEM of all cell lines within each group, control (C1–C4) and G2019S (GS1–GS3) (***$p \leq 0.001$ compared to the untreated cells). **e**–**j** Western-blot analyses of autophagy-related protein LC3-II in fibroblasts treated with U0126 (**e**, **f**), Atg5 siRNA (**g**, **h**) or LRRK2 siRNA (**i**, **j**). **e**, **g**, **i** Representative blots probed in the C1 and GS2 cell lines, with antibodies against LC3-II and GAPDH (used as a loading control under the same conditions). **f**, **h**, **j** The densitometry of each band, expressed in arbitrary units for each Western-blot analysis (***$p \leq 0.001$ compared treated and untreated cells). **k** The detection of PI-positive cells. Fibroblasts were treated with 20 μM U0126 for 24 h, transiently transfected with Atg5 siRNA or LRRK2 siRNA, followed by staining with PI to determine the viable cells. Data are expressed as the mean ± SEM of all cell lines within each group, control (C1–C4) and G2019S (GS1–GS3). (***$p \leq 0.001$, **$p \leq 0.01$ between the treated and untreated cells)

cells via the decrease in autophagy. To investigate the role of ERK inhibition, we induced autophagy inhibition with Atg5 siRNA (an essential protein for autophagy) in parallel. Atg5 knockdown produced a significant decrease of LC3-II in both cell types (Fig. 6g, h), as expected. While control cells exhibited an increase in cell death, a reduction in cell death was observed in *G2019S* LRRK2 mutant fibroblasts (Fig. 6k). Thus, in both cell types, MEK/ERK inhibition and the specific genetic inhibition of autophagy resulted in the same behavior. In another experiment, we evaluated the effect of LRRK2 siRNA knockdown on autophagy and cell sensitivity. LRRK2 knockdown induces a significant increase in LC3-II in both cell types (Fig. 6i, j) and an increase in cell death in both cell types (Fig. 6k).

Discussion

The deregulation of autophagy has been associated with the modulation of the activities of the LRRK2 protein, especially its kinase activity. The LRRK2 protein is involved in cellular autophagy through direct modulation, alteration of its own kinase activity, or the mediation of autophagy in response to external stimuli. The LRRK2 protein is therefore essential for maintaining the equilibrium between cellular degradation and synthesis.

In our study, we used human fibroblasts, a suitable model to study this process [49] that has previously been employed in the study of other PD-related proteins such as parkin and PINK1 [53]. We demonstrate the relationship between the *G2019S* LRRK2 mutation and autophagy.

Our results demonstrate that fibroblasts with the *G2019S* LRRK2 mutation show higher levels of basal autophagy compared to control cells.

In this model, when autophagosome–lysosome fusion was blocked with Baf A1, there was an arrest of autophagic flux and an increase in cell death in fibroblasts with and without the *G2019S* LRRK2 mutation. However, as *G2019S* LRRK2 cells have higher basal levels of autophagy, Baf A1 induces a greater accumulation of material that must be degraded in the mutant cells, thus leading to higher cell death in *G2019S* LRRK2 cells than in control cells treated with Baf A1. Furthermore, under starvation conditions, we observed an increase in cell death in both cell types; thus, differences in basal autophagy due to the *G2019S* LRRK2 mutation (mTOR-independent) and autophagy induced by starvation (mTOR-dependent) are independent of one another.

Many studies have described the participation of MEK/ERK route in autophagy [54], and this route have been documented as LRRK2 substrates [44]. In fact, in our model, the levels of ERK1/2 phosphorylation are increased in *G2019S* LRRK2 cells when compared to control cells. We show that U0126, a pharmacological inhibitor of MEK/ERK pathway, reduced the heightened levels of autophagy observed in cells with the *G2019S* LRRK2 mutation and increased autophagy in control cells. This phenomenon has been observed in other studies [17] and corroborates the importance of the MEK/ERK route in the basal autophagy of the control cells as well as in the exacerbated autophagy observed in mutant cells. Moreover, after the use of U0126, the cell sensitivity observed in *G2019S* LRRK2 cells was reduced; however, in control cells, apoptotic hallmarks increased.

Moreover, when we blocked the formation of autophagosomes with Atg5 siRNA, we observed the same results as when U0126 was used. In this sense, we observed a decrease in autophagy levels in both cell types, however in control cells results an increase of cell sensitivity, but G*2019S* LRRK2 mutant fibroblasts was accompanied by a decrease in death parameters in mutant cells. Therefore, it is possible to establish a correlation between autophagy via MEK/ERK and changes in cell sensitivity. In control cells, cell sensitivity increased after the use of U0126 or Atg5 siRNA due to changes in essential cell maintenance mechanisms. The blockage of the MEK/ERK route by U0126 inhibits one survival pathway of great importance in the cells and the use of Atg5 siRNA in control cells induces an inhibition of basal autophagy, which induces cell damage. On the other hand, we can confirm that exacerbated autophagy induced by MEK/ERK route in *G2019S* LRRK2 fibroblasts is inducing a negative effect on the cell, that are eliminated, either U0126 treatment or ATG5 siRNA, reducing this sensitivity.

As observed in other studies [50], LRRK2 knockdown induced increased autophagy and death in both cell types. This fact is important because the cell sensitivity exhibited by *G2019S* mutant cells was only reverted when aberrant autophagy was blocked (with Atg5 siRNA) or the LRRK2 substrate implicated in this process was blocked (with U0126). However, when we blocked the total LRRK2 protein expression, the behavior observed in the mutant cells was the same as that observed in the control cells. This result confirms that the importance of the presence of the *G2019S* LRRK2 mutation remains in the increased kinase activity and consequent overactivation of MEK/ERK pathway; when LRRK2 protein expression is abrogated, cell damage and increased levels of autophagy occur in both cell types in the same manner. In summary, the damage induced by the exacerbated autophagy levels observed in the mutant cells is not a direct consequence of the LRRK2 protein but is due to excess kinase activity that overactivates the MEK/ERK route, resulting in a negative effect in mutant cells.

The defensive or protective autoregulatory mechanism that accelerates the degradation of misfolded proteins may explain the increased number of autophagic vacuoles in the

brains of PD patients [27, 55]. However, many authors consider this autophagic flux to be a critical contributing factor in the induction of cell death [29]. It is important to elucidate the specific mechanism that produces increased autophagy levels that are MEK/ERK dependent. Autophagy levels in *G2019S* LRRK2 fibroblasts could be exacerbated as a direct result of LRRK2 activity or may be an indirect effect of misfolded proteins/aggregates. Indeed, in this model, we observed higher levels of alpha-synuclein in *G2019S* LRRK2 mutant fibroblasts (data not shown). Many studies have shown that the *G2019S* LRRK2 mutation induces alpha-synuclein aggregation, initiating and enhancing the formation of alpha-synuclein aggregates [56]. In 2009, Lin et al. reported that LRRK2 accelerates the progression of neuropathological abnormalities, proposing a link between alpha-synuclein and LRRK2 in the development of neurodegeneration [57, 58]. Some studies indicate that LRRK2 phosphorylates alpha-synuclein (Ser129) [59], resulting in the overexpression of this protein [60]. Moreover, this interaction may occur via the extracellular signal-regulated kinase pathway [45], although the mechanisms remain unknown [55, 61, 62]. Therefore, further investigation is needed to understand whether the *G2019S* LRRK2 mutation induces the accumulation of certain proteins such as alpha-synuclein and whether this accumulation exacerbates the basal levels of autophagy, resulting in toxicity to the cell, or whether the exacerbated autophagy is induced directly via MEK/ERK.

In conclusion, the present study demonstrates that the inhibition of the MEK/ERK route results in a reversal of sensitivity in cells with the *G2019S* mutation by reducing aberrant autophagy and apoptosis in the mutant cell line. This finding may inspire new research on the etiology of PD to further investigate this interaction. Further work is necessary to determine how MEK/ERK-dependent LRRK2-mediated autophagy affects stress and neurodegeneration in PD and the mechanisms involved in this process. The present study is an initial step in understanding the mechanisms of autophagy deregulation and may aid in future research that aims to control sensitivity and prevent cell death in cells with the *G2019S* LRRK2 mutation.

Acknowledgments The authors would like to thank P. Delgado, R. Ronco, S.M.S.Y. Diop, V. Llorente-Vera, J. Bragado, J. Correa, R. Tarazona, and R. Rodriguez for invaluable technical assistance. The authors also thank FUNDESALUD. José M. Bravo-San Pedro was supported by a Junta de Extremadura predoctoral fellowship. Mireia Niso-Santano was supported as a postdoctoral researcher by the University of Extremadura. Ruben Gómez-Sánchez was supported by a Spanish Ministerio de Educación predoctoral fellowship. Ana Aiastui-Pujana and Ana Gorostidi were supported by the Ilundain Fundazioa. Rosa-Ana González-Polo was supported by a "Miguel Servet" contract (ISCIII, Ministerio de Ciencia e Innovación, Spain). Dr. Sánchez-Pernaute received research support from the Ministerio de Ciencia e Innovación, Spain (SAF 2008-04615). Dr. López de Munain received research support from the Basque Government, Spain (SAIOTEK SA-2009/00071). Dr. González-Polo received research support from ISCIII (Ministerio de Ciencia e Innovación, Spain (CP0800010, PI11/0040) and FUNDESALUD (PRIS11014). Dr. José M. Fuentes received research support from the Ministerio de Ciencia e Innovación, Spain (SAF2010-14993), FUNDESALUD (PRIS10013, PRIS11019), CIBERNED (CB06/05/004) and Consejería, Economía, Comercio e Innovación Junta de Extremadura (GRU10054).

Conflict of interest None.

References

1. Gerlach M, Riederer P (1996) Animal models of Parkinson's disease: an empirical comparison with the phenomenology of the disease in man. J Neural Transm 103:987–1041
2. Martinez-Vicente M, Cuervo AM (2007) Autophagy and neurodegeneration: when the cleaning crew goes on strike. Lancet Neurol 6:352–361
3. Gonzalez-Polo RA, Niso-Santano M, Ortiz–Ortiz MA, Gomez-Martin A, Moran JM, Garcia-Rubio L, Francisco-Morcillo J, Zaragoza C, Soler G, Fuentes JM (2007) Inhibition of paraquat-induced autophagy accelerates the apoptotic cell death in neuroblastoma SH-SY5Y cells. Toxicol Sci 97:448–458
4. Paisan-Ruiz C, Jain S, Evans EW, Gilks WP, Simon J, van der Brug M, Lopez de Munain A, Aparicio S, Gil AM, Khan N et al (2004) Cloning of the gene containing mutations that cause PARK8-linked Parkinson's disease. Neuron 44:595–600
5. Berg D, Schweitzer KJ, Leitner P, Zimprich A, Lichtner P, Belcredi P, Brussel T, Schulte C, Maass S, Nagele T et al (2005) Type and frequency of mutations in the LRRK2 gene in familial and sporadic Parkinson's disease. Brain 128:3000–3011
6. Ozelius LJ, Senthil G, Saunders-Pullman R, Ohmann E, Deligtisch A, Tagliati M, Hunt AL, Klein C, Henick B, Hailpern SM et al (2006) LRRK2 G2019S as a cause of Parkinson's disease in Ashkenazi Jews. N Engl J Med 354:424–425
7. West AB, Moore DJ, Biskup S, Bugayenko A, Smith WW, Ross CA, Dawson VL, Dawson TM (2005) Parkinson's disease-associated mutations in leucine-rich repeat kinase 2 augment kinase activity. Proc Natl Acad Sci USA 102:16842–16847
8. Greggio E, Jain S, Kingsbury A, Bandopadhyay R, Lewis P, Kaganovich A, van der Brug MP, Beilina A, Blackinton J, Thomas KJ et al (2006) Kinase activity is required for the toxic effects of mutant LRRK2/dardarin. Neurobiol Dis 23:329–341
9. Jaleel M, Nichols RJ, Deak M, Campbell DG, Gillardon F, Knebel A, Alessi DR (2007) LRRK2 phosphorylates moesin at threonine-558: characterization of how Parkinson's disease mutants affect kinase activity. Biochem J 405:307–317
10. Gillardon F (2009) Leucine-rich repeat kinase 2 phosphorylates brain tubulin-beta isoforms and modulates microtubule stability—a point of convergence in parkinsonian neurodegeneration? J Neurochem 110:1514–1522
11. Gandhi PN, Wang X, Zhu X, Chen SG, Wilson-Delfosse AL (2008) The Roc domain of leucine-rich repeat kinase 2 is sufficient for interaction with microtubules. J Neurosci Res 86:1711–1720
12. Imai Y, Gehrke S, Wang HQ, Takahashi R, Hasegawa K, Oota E, Lu B (2008) Phosphorylation of 4E-BP by LRRK2 affects the maintenance of dopaminergic neurons in *Drosophila*. EMBO J 27:2432–2443

13. Webber PJ, Smith AD, Sen S, Renfrow MB, Mobley JA, West AB (2011) Autophosphorylation in the leucine-rich repeat kinase 2 (LRRK2) GTPase domain modifies kinase and GTP-binding activities. J Mol Biol 412:94–110
14. Kamikawaji S, Ito G, Iwatsubo T (2009) Identification of the autophosphorylation sites of LRRK2. Biochemistry 48:10963–10975
15. Doggett EA, Zhao J, Mork CN, Hu D, Nichols RJ (2012) Phosphorylation of LRRK2 serines 955 and 973 is disrupted by Parkinson's disease mutations and LRRK2 pharmacological inhibition. J Neurochem 120:37–45
16. Dzamko N, Deak M, Hentati F, Reith AD, Prescott AR, Alessi DR, Nichols RJ (2010) Inhibition of LRRK2 kinase activity leads to dephosphorylation of Ser(910)/Ser(935), disruption of 14-3-3 binding and altered cytoplasmic localization. Biochem J 430:405–413
17. Plowey ED, Cherra SJ 3rd, Liu YJ, Chu CT (2008) Role of autophagy in G2019S-LRRK2-associated neurite shortening in differentiated SH-SY5Y cells. J Neurochem 105:1048–1056
18. Liou AK, Leak RK, Li L, Zigmond MJ (2008) Wild-type LRRK2 but not its mutant attenuates stress-induced cell death via ERK pathway. Neurobiol Dis 32:116–124
19. Meredith GE, Totterdell S, Petroske E, Santa Cruz K, Callison RC Jr, Lau YS (2002) Lysosomal malfunction accompanies alpha-synuclein aggregation in a progressive mouse model of Parkinson's disease. Brain Res 956:156–165
20. Smith WW, Pei Z, Jiang H, Moore DJ, Liang Y, West AB, Dawson VL, Dawson TM, Ross CA (2005) Leucine-rich repeat kinase 2 (LRRK2) interacts with parkin, and mutant LRRK2 induces neuronal degeneration. Proc Natl Acad Sci USA 102:18676–18681
21. Shin N, Jeong H, Kwon J, Heo HY, Kwon JJ, Yun HJ, Kim CH, Han BS, Tong Y, Shen J et al (2008) LRRK2 regulates synaptic vesicle endocytosis. Exp Cell Res 314:2055–2065
22. Ko HS, Bailey R, Smith WW, Liu Z, Shin JH, Lee YI, Zhang YJ, Jiang H, Ross CA, Moore DJ et al (2009) CHIP regulates leucine-rich repeat kinase-2 ubiquitination, degradation, and toxicity. Proc Natl Acad Sci USA 106:2897–2902
23. Levine B, Klionsky DJ (2004) Development by self-digestion: molecular mechanisms and biological functions of autophagy. Dev Cell 6:463–477
24. Kondo Y, Kondo S (2006) Autophagy and cancer therapy. Autophagy 2:85–90
25. Nakai A, Yamaguchi O, Takeda T, Higuchi Y, Hikoso S, Taniike M, Omiya S, Mizote I, Matsumura Y, Asahi M et al (2007) The role of autophagy in cardiomyocytes in the basal state and in response to hemodynamic stress. Nat Med 13:619–624
26. Gonzalez-Polo R, Niso-Santano M, Moran JM, Ortiz–Ortiz MA, Bravo-San Pedro JM, Soler G, Fuentes JM (2009) Silencing DJ-1 reveals its contribution in paraquat-induced autophagy. J Neurochem 109:889–898
27. Anglade P, Vyas S, Javoy-Agid F, Herrero MT, Michel PP, Marquez J, Mouatt-Prigent A, Ruberg M, Hirsch EC, Agid Y (1997) Apoptosis and autophagy in nigral neurons of patients with Parkinson's disease. Histol Histopathol 12:25–31
28. Baehrecke EH (2005) Autophagy: dual roles in life and death? Nat Rev Mol Cell Biol 6:505–510
29. Bursch W (2001) The autophagosomal–lysosomal compartment in programmed cell death. Cell Death Differ 8:569–581
30. Kroemer G, Marino G, Levine B (2010) Autophagy and the integrated stress response. Mol Cell 40:280–293
31. Reggiori F, Klionsky DJ (2002) Autophagy in the eukaryotic cell. Eukaryot Cell 1:11–21
32. Djavaheri-Mergny M, Amelotti M, Mathieu J, Besancon F, Bauvy C, Souquere S, Pierron G, Codogno P (2006) NF-kappaB activation represses tumor necrosis factor-alpha-induced autophagy. J Biol Chem 281:30373–30382
33. Pattingre S, Tassa A, Qu X, Garuti R, Liang XH, Mizushima N, Packer M, Schneider MD, Levine B (2005) Bcl-2 antiapoptotic proteins inhibit Beclin 1-dependent autophagy. Cell 122:927–939
34. Petiot A, Ogier-Denis E, Blommaart EF, Meijer AJ, Codogno P (2000) Distinct classes of phosphatidylinositol 3′-kinases are involved in signaling pathways that control macroautophagy in HT-29 cells. J Biol Chem 275:992–998
35. Gonzalez-Polo RA, Soler G, Alvarez A, Fabregat I, Fuentes JM (2003) Vitamin E blocks early events induced by 1-methyl-4-phenylpyridinium (MPP+) in cerebellar granule cells. J Neurochem 84:305–315
36. Sivaprasad U, Basu A (2008) Inhibition of ERK attenuates autophagy and potentiates tumour necrosis factor-alpha-induced cell death in MCF-7 cells. J Cell Mol Med 12:1265–1271
37. Wang J, Whiteman MW, Lian H, Wang G, Singh A, Huang D, Denmark T (2009) A non-canonical MEK/ERK signaling pathway regulates autophagy via regulating Beclin 1. J Biol Chem 284:21412–21424
38. Criollo A, Senovilla L, Authier H, Maiuri MC, Morselli E, Vitale I, Kepp O, Tasdemir E, Galluzzi L, Shen S et al (2010) The IKK complex contributes to the induction of autophagy. EMBO J 29:619–631
39. Pungaliya PP, Bai Y, Lipinski K, Anand VS, Sen S, Brown EL, Bates B, Reinhart PH, West AB, Hirst WD et al (2010) Identification and characterization of a leucine-rich repeat kinase 2 (LRRK2) consensus phosphorylation motif. PLoS One 5:e13672
40. Gomez-Suaga P, Luzon-Toro B, Churamani D, Zhang L, Bloor-Young D, Patel S, Woodman PG, Churchill GC, Hilfiker S (2012) Leucine-rich repeat kinase 2 regulates autophagy through a calcium-dependent pathway involving NAADP. Hum Mol Genet 21:511–525
41. Parisiadou L, Xie C, Cho HJ, Lin X, Gu XL, Long CX, Lobbestael E, Baekelandt V, Taymans JM, Sun L et al (2009) Phosphorylation of ezrin/radixin/moesin proteins by LRRK2 promotes the rearrangement of actin cytoskeleton in neuronal morphogenesis. J Neurosci 29:13971–13980
42. Lee JY, Koga H, Kawaguchi Y, Tang W, Wong E, Gao YS, Pandey UB, Kaushik S, Tresse E, Lu J et al (2010) HDAC6 controls autophagosome maturation essential for ubiquitin-selective quality-control autophagy. EMBO J 29:969–980
43. Andres-Mateos E, Mejias R, Sasaki M, Li X, Lin BM, Biskup S, Zhang L, Banerjee R, Thomas B, Yang L et al (2009) Unexpected lack of hypersensitivity in LRRK2 knock-out mice to MPTP (1-methyl-4-phenyl-1,2,3,6-tetrahydropyridine). J Neurosci 29:15846–15850
44. Gloeckner CJ, Schumacher A, Boldt K, Ueffing M (2009) The Parkinson disease-associated protein kinase LRRK2 exhibits MAPKKK activity and phosphorylates MKK3/6 and MKK4/7, in vitro. J Neurochem 109:959–968
45. Carballo-Carbajal I, Weber-Endress S, Rovelli G, Chan D, Wolozin B, Klein CL, Patenge N, Gasser T, Kahle PJ (2010) Leucine-rich repeat kinase 2 induces alpha-synuclein expression via the extracellular signal-regulated kinase pathway. Cell Signal 22:821–827
46. Gelb DJ, Oliver E, Gilman S (1999) Diagnostic criteria for Parkinson disease. Arch Neurol 56:33–39
47. Fuentes JM, Lompre AM, Moller JV, Falson P, le Maire M (2000) Clean Western blots of membrane proteins after yeast heterologous expression following a shortened version of the method of Perini et al. Anal Biochem 285:276–278
48. Pattingre S, Bauvy C, Codogno P (2003) Amino acids interfere with the ERK1/2-dependent control of macroautophagy by controlling the activation of Raf-1 in human colon cancer HT-29 cells. J Biol Chem 278:16667–16674
49. Mortiboys H, Johansen KK, Aasly JO, Bandmann O (2010) Mitochondrial impairment in patients with Parkinson disease with the G2019S mutation in LRRK2. Neurology 75:2017–2020

50. Alegre-Abarrategui J, Christian H, Lufino MM, Mutihac R, Venda LL, Ansorge O, Wade-Martins R (2009) LRRK2 regulates autophagic activity and localizes to specific membrane microdomains in a novel human genomic reporter cellular model. Hum Mol Genet 18:4022–4034
51. Noda T, Ohsumi Y (1998) Tor, a phosphatidylinositol kinase homologue, controls autophagy in yeast. J Biol Chem 273:3963–3966
52. Klionsky DJ, Elazar Z, Seglen PO, Rubinsztein DC (2008) Does bafilomycin A1 block the fusion of autophagosomes with lysosomes? Autophagy 4:849–950
53. Rakovic A, Grunewald A, Seibler P, Ramirez A, Kock N, Orolicki S, Lohmann K, Klein C (2010) Effect of endogenous mutant and wild-type PINK1 on Parkin in fibroblasts from Parkinson disease patients. Hum Mol Genet 19:3124–3137
54. Dagda RK, Zhu J, Kulich SM, Chu CT (2008) Mitochondrially localized ERK2 regulates mitophagy and autophagic cell stress: implications for Parkinson's disease. Autophagy 4:770–782
55. Eriksen JL, Wszolek Z, Petrucelli L (2005) Molecular pathogenesis of Parkinson disease. Arch Neurol 62:353–357
56. Kondo K, Obitsu S, Teshima R (2011) Alpha-synuclein aggregation and transmission are enhanced by leucine-rich repeat kinase 2 in human neuroblastoma SH-SY5Y cells. Biol Pharm Bull 34:1078–1083
57. Lin X, Parisiadou L, Gu XL, Wang L, Shim H, Sun L, Xie C, Long CX, Yang WJ, Ding J et al (2009) Leucine-rich repeat kinase 2 regulates the progression of neuropathology induced by Parkinson's-disease-related mutant alpha-synuclein. Neuron 64:807–827
58. Jellinger KA (2011) Interaction between alpha-synuclein and other proteins in neurodegenerative disorders. ScientificWorldJournal 11:1893–1907
59. Qing H, Wong W, McGeer EG, McGeer PL (2009) Lrrk2 phosphorylates alpha synuclein at serine 129: Parkinson disease implications. Biochem Biophys Res Commun 387:149–152
60. Tong Y, Shen J (2009) Alpha-synuclein and LRRK2: partners in crime. Neuron 64:771–773
61. Goedert M (2001) Alpha-synuclein and neurodegenerative diseases. Nat Rev Neurosci 2:492–501
62. Vekrellis K, Xilouri M, Emmanouilidou E, Rideout HJ, Stefanis L (2011) Pathological roles of alpha-synuclein in neurological disorders. Lancet Neurol 10:1015–1025